Generation of functionalized polymer nanolayer on implant surface via initiated chemical vapor deposition (iCVD)

ARTICLE *in* JOURNAL OF COLLOID AND INTERFACE SCIENCE · FEBRUARY 2015

Impact Factor: 3.37 · DOI: 10.1016/j.jcis.2014.10.018

Journal of Colloid and Interface Science 439 (2015) 34–41

Contents lists available at ScienceDirect

Journal of Colloid and Interface Science

www.elsevier.com/locate/jcis

Generation of functionalized polymer nanolayer on implant surface via initiated chemical vapor deposition (iCVD)

Se Woong Park [a], Donghyun Lee [a], Hak Rae Lee [b], Ho-Jin Moon [a], Bo Ra Lee [b], Wan-Kyu Ko [a], Su-Jin Song [a], Sang Jin Lee [a], Kwanwoo Shin [c], Wonhyeong Jang [c], Jin-Kyu Yi [d], Sung Gap Im [b,*], Il Keun Kwon [a,*]

[a] Department of Maxillofacial Biomedical Engineering and Institute of Oral Biology, School of Dentistry, Kyung Hee University, Seoul 130-701, Republic of Korea
[b] Department of Chemical and Biomolecular Engineering and KI for NanoCentury, Korea Advanced Institute of Science and Technology, Daejeon 305-701, Republic of Korea
[c] Department of Chemistry and Institute of Biological Interfaces, Sogang University, Seoul 121-742, Republic of Korea
[d] Department of Conservative Dentistry, School of Dentistry, Kyung Hee University, Seoul 130-701, Republic of Korea

ARTICLE INFO

Article history:
Received 26 May 2014
Accepted 14 October 2014
Available online 19 October 2014

Keywords:
Initiated chemical vapor deposition
Functional polymer
Implant
Surface treatment

ABSTRACT

Initiated chemical vapor deposition (iCVD) was utilized to generate a 200 nm thick, uniform, functionalized polymer nanolayer comprised of glycidyl methacrylate (GMA) on the surface of titanium implants as a means to improve cellular attachment. Dot-patterned GMA-coated specimens were prepared as well as fully coated specimens. *In vitro* cellular responses, including cell morphology, protein adsorption, cell proliferation assays, alkaline phosphate activity (ALP) assays, and calcium deposition assays were studied using adipose derived stem cells. The mechanical stability of the thin film was investigated by XPS and FE-SEM analysis of the GMA-coated implant after implantation to an extracted bone from a pig. The GMA-coated specimens displayed increased protein adsorption, higher alkaline phosphatase activities, and higher calcium deposition as compared to control sample with no cytotoxicity. Additionally, no defect was observed in the test of mechanical stability. Notably, dot-patterned GMA-coated samples displayed higher alkaline phosphatase activities than others. Functionalized polymer nanolayer deposition via iCVD is a flexible and robust technique capable of mass production of biocompatible layers. These properties make this technique very suitable for implant applications in a variety of ways.

1. Introduction

Titanium has been widely used as a biomaterial, especially in dental and orthopedic implants, due to its mechanical properties, resistance to corrosion, and excellent biocompatibility [1,2]. The surface properties of these implants, such as roughness, wettability, and surface charge, play a critical role in cell adhesion and ultimately osseointegration. This is crucial for the ultimate success of an implant. For increasing surface roughness, various methods such as grit-blasting, acid-etching, and anodization have been investigated [3,4]. Furthermore, various surface treatments for introducing hydrophilicity, antibacterial activity, and osteoconductivity have been studied [5–7].

Initiated chemical vapor deposition (iCVD), as reported by Gleason [8,9], is a facile method to deposit a variety of functional polymer nanolayers even on rough surfaces such as fabrics and surfaces with 7 μm trenches [7,10]. iCVD is a solvent-less and low-temperature radical polymerization technique, which can be utilized to make uniform nanolayers with high conformation [11], to synthesize copolymers [12], and to make stable and rigid cross-linked polymers by adding crosslinkers [13].

In this study, anodized titanium implants were deposited with a functional polymer nanolayer via iCVD technique. As shown in Fig. 1, this treatment created a three-layered structure, which is composed of a layer of poly(glycidyl methacrylate) (pGMA) on top of an anodized oxide layer with the base layer being Ti metal. To increase surface area and roughness, a rough titanium oxide layer was introduced by anodization with H_2SO_4. GMA was polymerized on the anodized Ti surface using *tert*-butyl peroxide (TBPO) as the initiator. This results in the formation of a pGMA nanolayer. GMA, containing an epoxy ring, provides a good binding site and allows for various functionalities to be incorporated through a ring-opening reaction of the glycidyl moiety [14–16]. In anticipation of increasing cell attachment with chemical

* Corresponding author at: Korea Advanced Institute of Science and Technology, Department of Chemical and Biomolecular Engineering and KI for NanoCentury, Daejeon 305-701, Republic of Korea. Fax: +82 42 350 3976. (S.G. Im). Kyung Hee University, Department of Maxillofacial Biomedical Engineering and Institute of Oral Biology, School of Dentistry, 26, Kyungheedae-ro, Dongdaemun-gu, Seoul 130-701, Republic of Korea. Fax: +82 2 960 1457 (I.K. Kwon).
E-mail addresses: sgim@kaist.ac.kr (S.G. Im), kwoni@khu.ac.kr (I.K. Kwon).

http://dx.doi.org/10.1016/j.jcis.2014.10.018
0021-9797/

interaction, ~200 nm of pGMA was introduced onto the rough oxide surface. These were then evaluated *in vitro* with adipose derived stem cells (ADSCs). ADSCs are easily accessible and abundant. Also ADSCs are similar to bone marrow stem cells in their differentiation potencies and have been widely applied in the tissue engineering field [17,18].

2. Materials and methods

2.1. Materials

Titanium disks (diameter: 12 mm, thickness: 1 mm) and fixtures (diameter: 4 mm, length: 10 mm) were supplied by Biotem Co., Ltd. (Busan, Korea). Glycidyl Methacrylate (97%) and tert-butyl peroxide (98%) for iCVD were purchased from Sigma–Aldrich. Bradford assay solution was purchased from Bio-Rad (Hercules, CA, USA). StemPro® Human ADSCs (adipose derived stem cells) and MesenPRO RS™ medium (MPRO medium) were obtained from Invitrogen (Carlsbad, CA, USA). Fetal bovine serum (FBS), penicillin, and streptomycin were purchased from GIBCO (Gran Island, NY). The other chemicals were purchased from Sigma–Aldrich.

2.2. Methods

2.2.1. Sample preparation

For the *in vitro* experimentation, three kinds of specimens were prepared (Fig. 1). For a control, a commercially used surface consisting of anodized Ti (**ANOD**) [19] was included. The test samples included fully pGMA coated (**GMA-full**) specimens and dot-patterned pGMA coated (**GMA-dot**) specimens.

2.2.2. Anodization of Ti disk

Ti disks and fixtures were washed 2 times and cleaned in an ultra-sonicator for 15 min using hexane, acetone, ethanol and distilled water sequentially prior to use.

Anodization of the Ti disks and fixtures was performed in 2.0 M H_2SO_4 aqueous solution in a glass chamber with a magnetic stirrer in an ice bath. The applied voltage was 150 V for 2 min with a direct current power supply system (EX750H, Takasago Ltd., Japan). Titanium plates were used as both a cathode and an anode. After anodization, Ti samples were washed with water 3 times and then sonicated for 20 min followed by drying at 60 °C [20].

2.2.3. Polymer nanolayer deposition by iCVD

Glycidyl Methacrylate (GMA) and tert-butyl peroxide (TBPO) initiator were purchased and used without further purification. The polymerization took place in a custom-built iCVD reactor described previously [21] (Daeki Hi-Tech Co., Ltd). To deposit the iCVD pGMA films, the GMA monomer was heated to a temperature of 35 °C and vapor was fed into the reactor at a flow rate of 1.9 sccm. TBPO vapors (room temperature) were fed into the reactor via metering valves at a flow rate of 0.8 sccm. For the pure pGMA film, only GMA and TBPO were fed into the reactor concurrently with a reactor pressure of 200 mTorr. The substrate was kept at a temperature of 25 °C to promote monomer adsorption, and the filament temperature was maintained at 200 °C. For a dot-patterned deposition, a dot-patterned stainless steel mask (diameter:

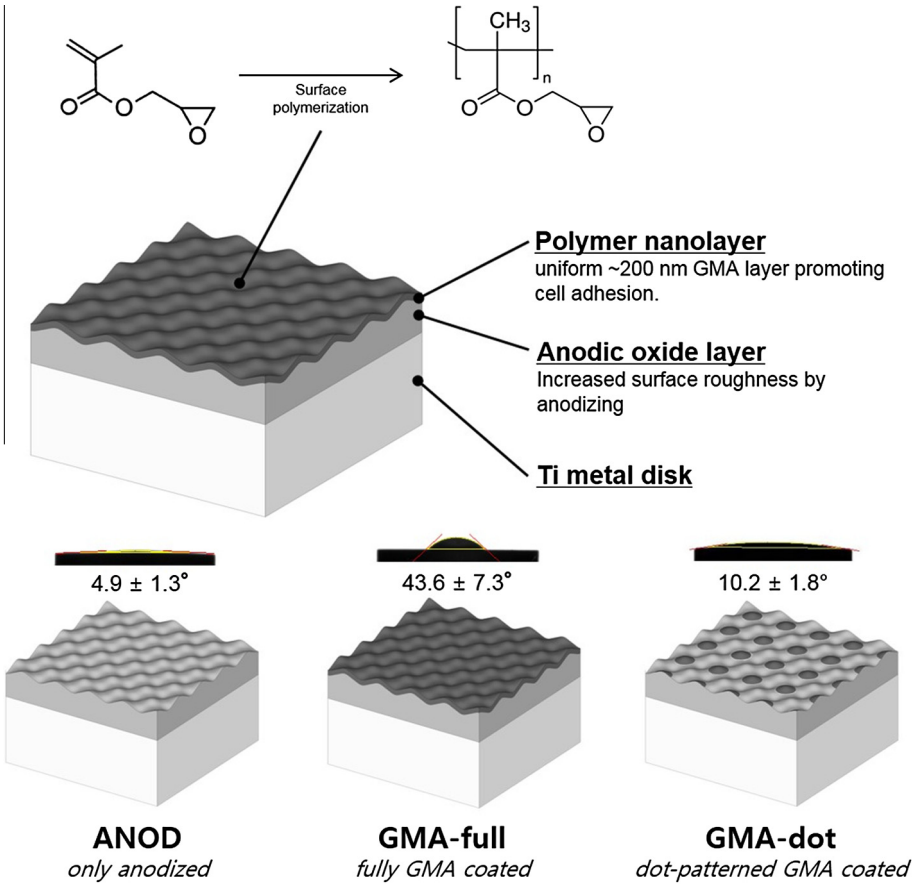

Fig. 1. Three-layered structure (upper) composed of a titanium metal base, an anodic oxide layer and a functional polymer nanolayer. Glycidyl methacrylate is polymerized on the surface of the oxide layer. **ANOD** is covered only with an anodized surface, **GMA-full** is coated with GMA fully and **GMA-dot** is coated with dot-patterned GMA over the anodized surface.

1 mm, center-to-center: 1.5 mm, Yesung, Korea) was placed on the prepared Ti disks. The geometrical area of the dot-pattern is *ca.* 40% of the total area of the metal mask.

2.2.4. Surface image and characterization

Field emission scanning electron microscope (FE-SEM) was utilized to observe the surface of the specimens using a LEO supra 55, Genesis 2000 (Carl Zeiss, Germany) at an acceleration voltage of 10 kV. Sputter coating was not needed. Atomic force microscope (AFM) images and roughness values of the surface were obtained by an Autoprobe CP system (Park Science, Sunnyvale, CA) used in non-contact mode under ambient conditions. X-ray Photoelectron Spectroscopy (XPS) was performed using a K-Alpha (Thermo Electron, UK) to characterize the GMA-coated surfaces.

Fourier Transform Infrared spectroscopy imaging (imaging IR) of **GMA-dot** was measured with a Cary 600 Series FTIR Microscope (Agilent Technologies, CA) equipped with a 16×16 pixel focal plane array (FPA) detector. IR Imaging data was accumulated in reflection mode at a resolution of 32 cm^{-1} in the range of 4000–900 cm^{-1} averaging 32 scans. Images of the dot-patterned stainless steel mask and GMA-dot were photographed with Sony NEX-F3.

2.2.5. Protein adsorption assay

Bovine serum albumin (BSA) was used as a representative protein for the protein adsorption assay [22]. Each surface was first wetted with 500 μl of PBS and then 500 μl of BSA (3 mg/ml PBS) was added onto each surface. After 24 h, non-adsorbed proteins were collected. The solution was diluted and tested using a Bradford assay solution (Bio-Rad, Hercules, CA, USA) to determine the amount of residual protein. The Bradford assay was performed according to the manufacturer's protocol. The resulting absorbance was measured at a wavelength of 595 nm using a microplate reader.

To identify chemical bonds between the GMA thin film and the BSA, FT-IR measurements were performed with Bruker Alpha FT-IR spectrometer (Bruker, MA). FT-IR spectra were recorded in the range of 4000–400 cm^{-1}. After GMA was polymerized on glass slides, the resultant films were immersed in PBS or BSA solution (3 mg/ml PBS) for 24 h. After drying, the films were exfoliated with a cutter. The reference FT-IR spectrum of the BSA was obtained directly with powder BSA and the sample FT-IR spectra were obtained with the exfoliated polymer thin films.

2.2.6. In vitro cellular responses

StemPro® Human ADSCs (adipose derived stem cells) were used to characterize the biocompatibility of each sample by measuring cell proliferation, alkaline phosphatase activity, and alizarin red staining. ADSCs were cultured in MesenPRO RS™ medium (MPRO medium, Invitrogen). Osteogenic medium consisting of dulbecco's modified eagle medium (DMEM) containing 15% fetal bovine serum (FBS, GIBCO), 100 U/ml penicillin (GIBCO), 100 μg/ml streptomycin (GIBCO), 10 mM β-glycerol phosphate disodium salt hydrate (Sigma–Aldrich, St. Louis, MO), 300 μM ascorbic acid (Sigma–Aldrich) and 0.1 μM dexamethasone (Sigma–Aldrich) was added. Prior to cell-seeding, the prepared specimens were sterilized with 70% EtOH for 10 min and rinsed twice with phosphate-buffered saline (PBS).

2.2.7. Cytotoxicity assay

ADSCs were seeded at a density of 2×10^4 cells/ml on the surface of the prepared Ti disks in 24-well plates and incubated in non-osteogenic media for 48 h. At predetermined time intervals (24 h and 48 h), specimens were rinsed with PBS and the CCK-8 proliferation kit reagents (Dojindo, Kumamoto, Japan) were added to each specimen. After 2 h of incubation, reagents were carefully transferred to 96-well plates. The optical density was measured using a microplate reader at a wavelength of 450 nm.

2.2.8. Alkaline phosphatase (ALP) activity assay

To estimate the osteogenic activity, the level of alkaline phosphatase (ALP) activity was measured. The cells were incubated in osteogenic media at 37 °C in 5% CO_2 and were cultured for 7 and 14 day (2×10^4 cells/ml, 24-well plate). At each predetermined time interval, the cell-seeded wells were washed with DPBS twice and then lysed using 1× RIPA buffer (50 mM Tri-HCl (pH 7.4), 150 mM NaCl, 0.25% deoxycholic acid, 1% NP-40 and 1 mM EDTA) along with a protease inhibitor cocktail (Boehringer Mannheim GmbH, Germany) for 30 min on ice. Each of the lysates was centrifuged at 1.3×10^4 rpm at 4 °C for 15 min to remove cellular debris. After centrifugation, the supernatant was collected and reacted with p-nitrophenol phosphate solution (pNPP, Sigma) in a 5% CO_2 humidified incubator at 37 °C for 30 min. The reaction with pNPP was then terminated by adding 50 μl of 1 M NaOH. The production of p-nitrophenol was measured by measuring the light absorption at 405 nm using a micro-plate reader. A calibration curve was generated using standard p-nitrophenol solutions. The concentration of produced total p-nitrophenol from cultured cells was calculated by comparing the obtained absorbances with the calibration curve. Finally, the enzymatic activity was expressed as μM of reaction product (p-nitrophenol) per minute per μg of total cellular protein.

2.2.9. Calcium deposition assay

ADSCs (at a density of 2×10^4 cells/well) were seeded on the surface of the prepared Ti disks, and incubated for 3 and 4 weeks respectively in osteogenic medium. At each of the predetermined time intervals, the cell-seeded wells were washed with DPBS twice, fixed for 20 min using 3.7% formaldehyde, and then washed with DPBS again. All the cells were stained in an incubator at 37 °C under 5% CO_2 for 1 h using 40 mM alizarin red staining solution (pH 4.2). The staining solution was removed after 1 h, washed with distilled water three times. For a quantitative analysis, the stained cells were desorbed with 10% 1-hexadecylpyridinium chloride and the absorbance was measured by using a microplate reader at 540 nm.

2.2.10. Observation of cell morphology

Cell shapes on the treated surface were observed using confocal laser scanning microscopy (CLSM, Eclipse E600W, Nikon, Tokyo, Japan). ADSCs were incubated for 7 days on the surfaces of the samples in non-osteogenic media in an incubator at 37 °C under 5% CO_2. The cultured cells on the samples were then washed with PBS three times and were fixed with 3.9% formaldehyde for 12 h. Subsequently, these were washed with PBS again and were stained with 1 ml of 0.5 wt% of oregon green 514 phalloidin and 0.1 wt% of DAPI. In order to measure the aspect ratio, Three to five photographs that did not contain too many cells and in which most of the cells were discriminable were selected. The major axes and minor axes of all the cells in the photographs were measured manually (n = 100) [23].

2.2.11. Thin film mechanical stability

Mechanical stabilities of the thin films were investigated by implantation into a bone extracted from a deceased pig. After implant sockets were prepared using a lance drill and a series of pilot drills (2 mm, 3.3 mm, and 3.8 mm) in sequence operated at 800 rpm using a micromotor (Impanteo, Anthogyre, Sallanches, France), the GMA-coated fixtures were implanted at 20 rpm with 50 N cm of torque. The fixtures were then removed and were characterized using FE-SEM (LEO supra 55, Genesis 2000, Carl Zeiss, Germany) and XPS (K-Alpha Thermo Electron, UK). XPS analysis was performed at six random spots on each fixture.

2.2.12. Statistical analysis

At least three samples for each experimental condition were used. Statistical comparisons were carried out using one-way ANOVA tests. Statistically significant values are defined as $^{*}P < 0.05$.

3. Results and discussion

3.1. Contact angle

Contact angles of water were measured for the **ANOD**'s surface, the **GMA-full**'s surface, and the **GMA-dot**'s surface. The **ANOD** displayed a super-hydrophilic characteristic (contact angle: 4.9 ± 1.3°), while **GMA-full** displayed a less hydrophilic surface (contact angle: 43.6 ± 7.3°). Hydrophilicity is closely related to cell differentiation [24,25]. Thus, in order to combine the super-hydrophilic surface and the GMA surface which has a cell binding property, **GMA-dot** was generated by coating the surface with a dot-patterned GMA. The **GMA-dot** showed a lower contact angle (contact angle: 10.2 ± 1.8°) than the **GMA-full** indicating improved hydrophilicity.

3.2. Surface imaging and characterization

Fig. 2 shows FE-SEM photographs of **ANOD**, and **GMA-full**. **ANOD**, which was anodized in H_2SO_4 at 150 V, has a rough oxide surface consisting of numerous open pores which leads to an increased surface area and increased roughness. The thickness of the oxide layer is ~2 μm, which was confirmed by cross sectional SEM via a focused ion beam (data not shown.). As shown in Fig. 2(b), after being coated with GMA via iCVD, the surface retained its roughness due to high conformity of the iCVD layer technique. There was little difference between the two surface morphologies. The GMA-coated surface is slightly darker than the non-coated surface due to the polymer thin film layer.

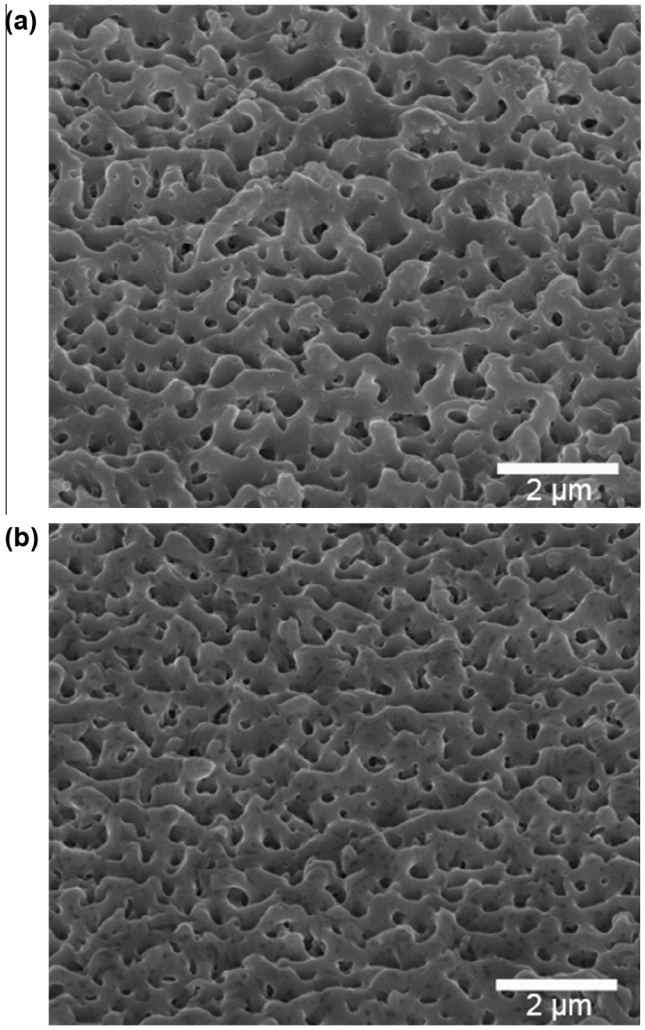

Fig. 2. FE-SEM micrograph of the anodic oxide layer surface of (a) **ANOD** and (b) **GMA-full**.

GMA-dot samples were prepared with a dot-patterned metal mask (Fig. 3(a)). The diameter of the dot-pattern is 1 mm and the distance between centers of dots is 1.5 mm. Fig. 3(b) shows a photograph of the resulting **GMA-dot**. The dot-pattern on the anodized substrate was successfully fabricated, but thick boundaries were formed due to infiltration of GMA monomer vapor into gaps between the metal mask and the substrate. Fig. 3(c) shows IR imaging of the boundary between the GMA polymer film and the substrate. Because GMA polymer film has peaks at 3000 cm^{-1} due to their alkyl groups, these images were collected at 3000 cm^{-1}. The area of the GMA film showed higher intensities (red color) than the substrate (blue color). The boundary (green color) between the GMA polymer film and the substrate was observed also in the IR image.

Fig. 4 shows three-dimensional surface images of pristine Ti, **ANOD**, and **GMA-full**, obtained from atomic force microscopy. While pristine Ti showed a relatively flat surface morphology, **ANOD** and **GMA-full** showed rough morphologies. Significant

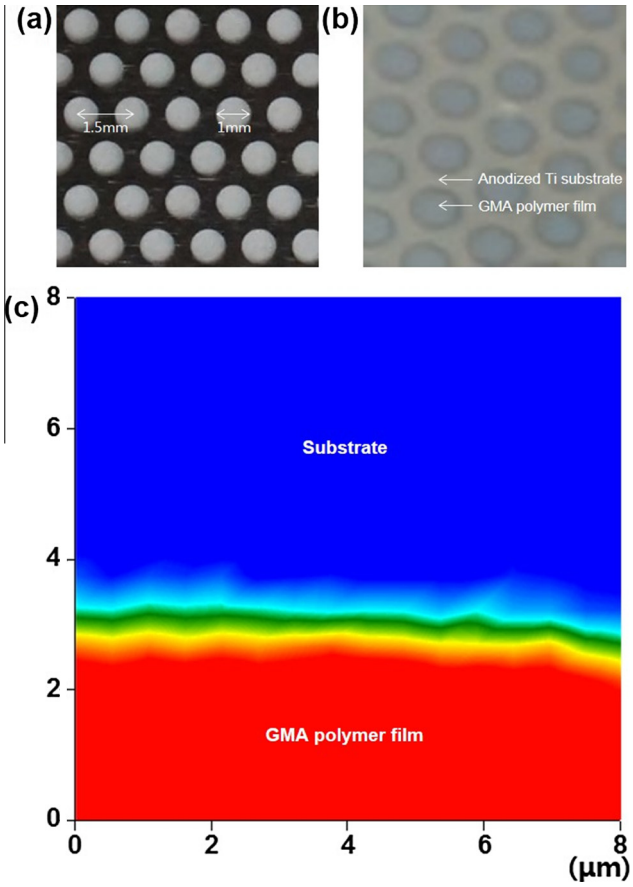

Fig. 3. Preparation of **GMA-dot**. (a) a metal mask for preparing **GMA-dot.** (b) Dot-patterned poly GMA on the **ANOD.** (c) 2-D FT-IR image of boundary between the GMA polymer film (red) and the substrate (blue) at 3000 cm^{-1}. (For interpretation of the references to colour in this figure legend, the reader is referred to the web version of this article.)

differences of surface morphology were not observed quantitatively between **ANOD** and **GMA-full**. Average roughness (R_a) was measured to be 100.3 nm, 168.0 nm, and 158.6 nm, respectively. Obviously, R_a values could not sufficiently describe the roughness of the nanostructure of the anodized surface. However, as shown in SEM images (Fig. 2), mesoporous structures of the anodized surfaces were maintained after GMA polymer films were deposited.

X-ray photoelectron spectroscopy was used to chemically analyze the pGMA thin films on the titanium substrate. Fig. 5 shows XPS spectra of **ANOD** and **GMA-full**. The XPS spectrum of **ANOD** shows peaks of Ti 2p and O 1s. The spectra of **GMA-full** shows O 1s, C 1s, and decreased Ti 2p peaks. These results suggest that the organic layer is formed on the surface and the layer covers the anodic oxide surface well. Though iCVD technique has good coverage for making polymer thin films, the entire surface of the anodized layer was not entirely covered due to the complicated structures of mesoporous anodized thin films.

To confirm the formation of peptide bonds between GMA polymer thin films and protein, FT-IR analyses of unexposed GMA film, a GMA film after immersion in PBS, a GMA film after immersion in BSA solution, and pure BSA powder were performed (Fig. 6). GMA polymer films shows peaks corresponding to epoxy groups (760, 847, and 908 cm^{-1}), C—O stretching (1250 cm^{-1}), C═O stretching (1725 cm^{-1}), and alkyl groups (2935–3000 cm^{-1}). BSA protein shows peaks corresponding to amide II (N—H, 1508 cm^{-1}), amide I (C═O, 1638 cm^{-1}), and N—H & O—H stretching. The unexposed GMA film and the GMA film after immersion in PBS show almost the same FT-IR spectra, which suggests that PBS does not have any effects on GMA polymer thin films. The GMA film immersed in BSA solution shows both peaks for the GMA film and the BSA. Furthermore, the GMA film immersed in BSA solution shows different peak intensities compared with the GMA film and the BSA. Especially, the GMA film immersed in BSA solution shows increased peak intensities around 3000 cm^{-1} and slightly shifted and increased peaks at 1645 cm^{-1}. This suggests that new bonds between the GMA polymer and the BSA protein were formed via ring opening of epoxy groups in the GMA polymer. The epoxy groups in the GMA polymer could bind to amino groups at N-terminal of the proteins, carboxylic acid groups at C-terminal of the proteins, and other site of the proteins by non-specific adhesions. These bindings between the GMA polymer and the protein contributed to the changes in the FT-IR spectrum. This result could be evidence that cells and cellular attachment proteins can chemically bind to the GMA polymer thin film.

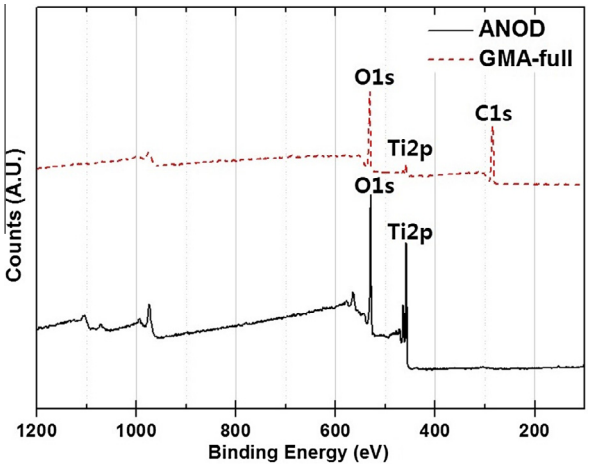

Fig. 5. XPS spectra of **ANOD** and **GMA-full**.

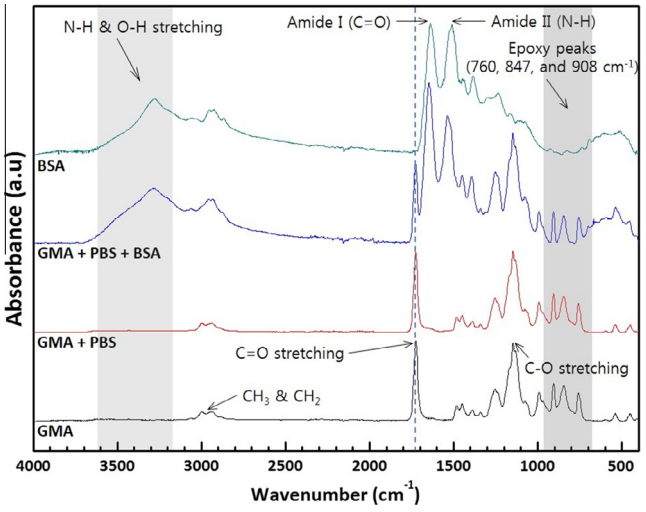

Fig. 6. FT-IR spectra of GMA, GMA after immersion in PBS for 24 h, GMA after immersion in BSA solution, and pure BSA.

3.3. Protein adsorption assay

To evaluate the adhesion abilities of GMA polymer thin films, the amounts of adsorbed BSA on each substrate were measured. The amount of adsorbed BSA showed a statistically significant increase in both the **GMA-full** and **GMA-dot** as compared with the **ANOD** and the **pristine Ti** substrate. Additionally the **GMA-full** showed a higher degree of adsorption than the **GMA-dot** as shown in Fig. 7(a). Because GMA-full has a more highly coated surface than GMA-dot, the GMA-full shows a larger amount of protein

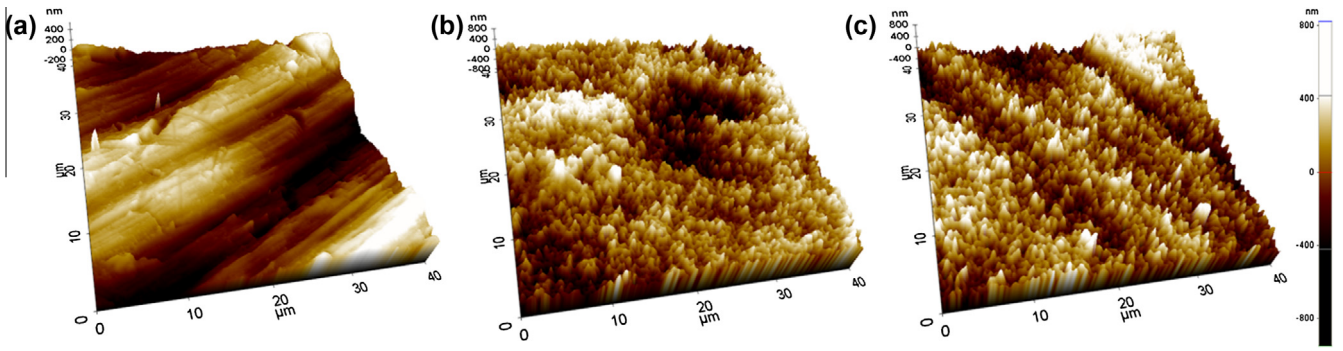

Fig. 4. Three-dimensional images of (a) Pristine Ti, (b) **ANOD**, and (c) **GMA-full** obtained from atomic force microscopy. Average values of roughness are 100.3 nm, 168.0 nm, and 158.6 nm, respectively.

adsorption. These results indicate that the functional groups of GMA adhere strongly to proteins.

3.4. Cytotoxicity assay

To investigate the effects of polymer GMA on cell cytotoxicity, we performed cytotoxicity assays on pristine Ti, **ANOD**, **GMA-full,** and **GMA-dot** using ADSCs with non-osteogenic media. The cytotoxicity assays using the ADSCs showed no significant difference on the surface of all specimens after 24 and 48 h of incubation (Fig. 7(b)). The pGMA deposited surface did not affect the cell cytotoxicity of ADSCs as compared with the anodized TiO_2 surface.

3.5. Alkaline phosphatase (ALP) activity assay and calcium deposition assay

Alkaline phosphatase has been widely used as an early marker of osteoblast differentiation. To identify the effects of the treated surfaces on the differentiation of the stem cells, the ALP activity was investigated after 1 and 2 weeks of incubation using osteogenic media on the surfaces of **ANOD**, **GMA-full** and **GMA-dot**. As shown in Fig. 7(c), the **GMA-dot** surface showed approximately 2 times higher ALP activities than that of **ANOD** and **GMA-full** both for 1 and 2 weeks of incubations. **GMA-full** showed higher ALP activity than that of **ANOD**, but the difference was not significant. It is already well-known that hydrophilic and rough surfaces increase ALP activities and encourage cell differentiation to osteoblast cells [24,26–29]. However, it is obvious that not only surface energy, but also chemical interactions are affecting the cell adhesion and differentiation.

As shown in FT-IR analyses of Fig. 6, even though the pGMA surface has less hydrophilicity, the surface presents chemically active sites via the epoxy rings. **GMA-dot** is composed of approximately 60% of the super-hydrophilic anodized surface and 40% of dot-patterned GMA functional polymers which acts to increase the adhesion of proteins. **GMA-dot** is more hydrophilic than **GMA-full** and also has epoxy groups that present cell-binding sites at the same time. Increasing the cell binding ability is not just increasing adhesion itself, but also promoting cell differentiation via $\alpha 2\beta 1$ integrin signaling in osteoblasts on the substrate surface and Dkk2 paracrine secretions [27,30]. Further studies are required regarding the exact chemical interactions between GMA coated surfaces and the osteoblast cell differentiation.

Fig. 7(d) shows Alizarin red-based calcium deposition assay of ADSCs cultured on **ANOD**, **GMA-full** and **GMA-dot** after 3 and 4 weeks of incubation with osteogenic media. While the ALP activity assay is used for evaluating early markers for bone differentiation, the calcium deposition assay is used to indicate late-stage differentiation of osteoblasts. The GMA coated specimens displayed a higher mineralization than the non-coated **ANOD** surface. Although the **GMA-dot** surface showed a much higher ALP activity, the total number of cells on the **GMA-dot** surface was relatively less than that on other specimens. The total amounts of calcium deposition were similar for both **GMA-full** and **GMA-dot**. Similar phenomena were found in previously reported literature [27,31]. They mentioned that the subsequent induction of genes associated with matrix maturation and mineralization were closely related with the decline in proliferative activity.

3.6. Cell morphology and aspect ratio

Fig. 8 shows morphologies of ADSCs on the pristine Ti, **ANOD**, and **GMA-full**. The stem cells were seeded on the surfaces and incubated during 7 days in non-osteogenic media. The cells grown

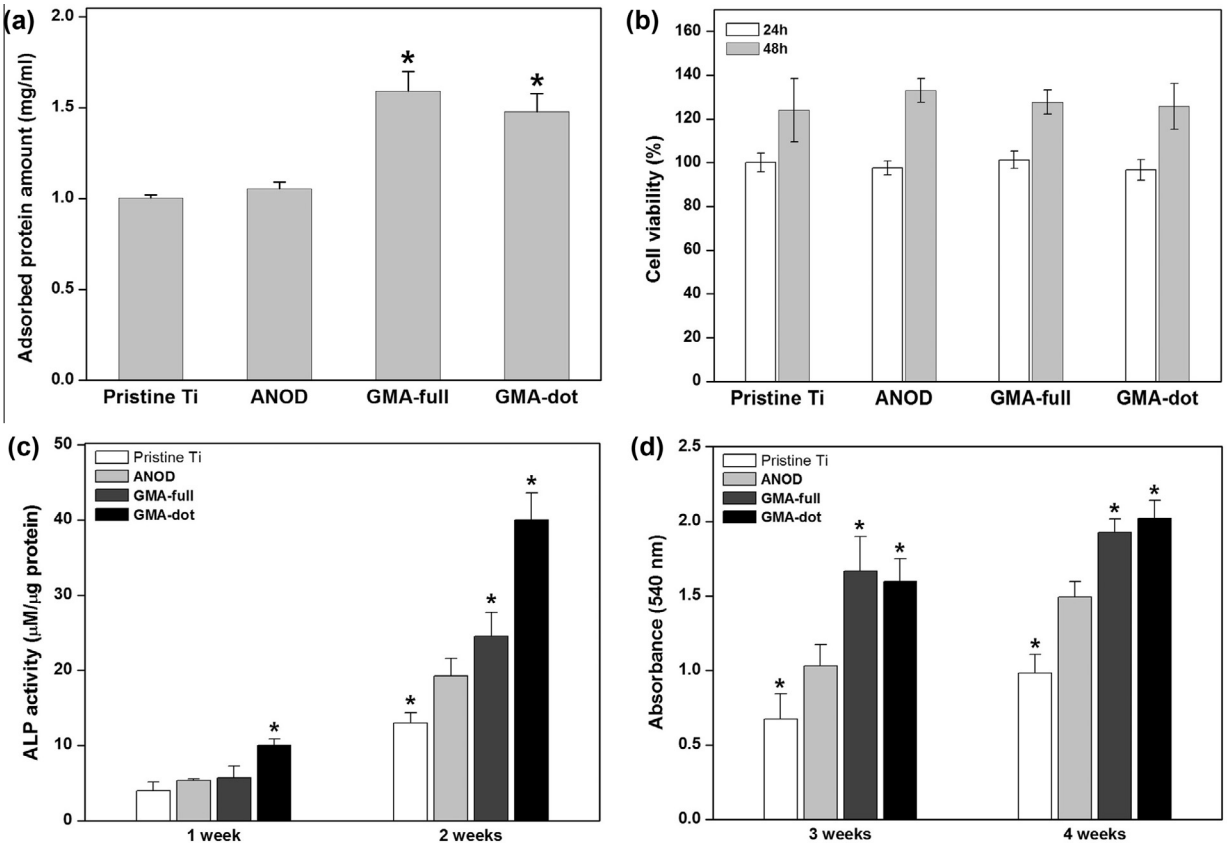

Fig. 7. *In vitro* test (a) protein adsorption assay, (b) cytotoxicity assay, (c) ALP activity assay and (d) calcium deposition assay. *$P < 0.05$ compared with **ANOD**.

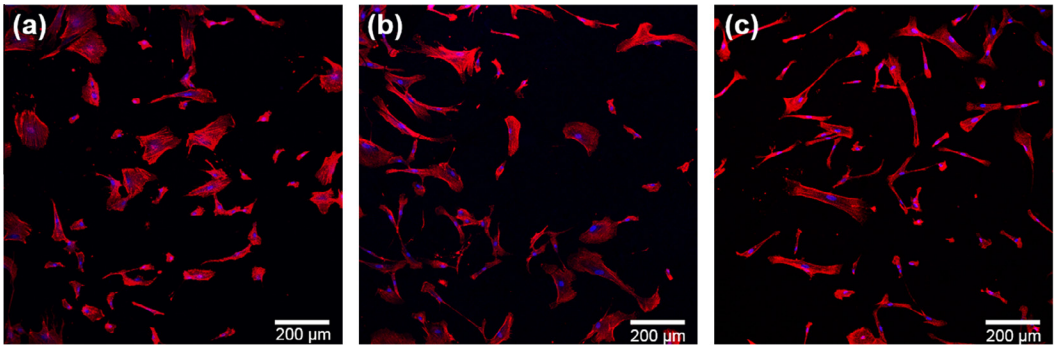

Fig. 8. Images of ADSCs cultured for 7 days stained with oregon green 514 phalloidin and DAPI on (a) pristine Ti, (b) **ANOD** and (c) **GMA-full** using confocal laser scanning microscopy.

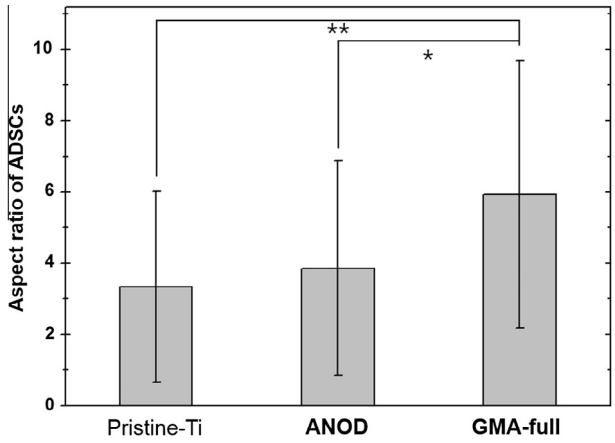

Fig. 9. Aspect ratio of ADSCs on (a) pristine Ti (b) **ANOD** (c) **GMA-full** ($n = 100$). $^{*}P < 10^{-4}$, $^{**}P < 10^{-6}$.

on the surface of **GMA-full** displayed relatively longer morphologies than those grown on the surface of pristine Ti and **ANOD**. For quantitative measurement, major axis and minor axis of discriminable cells were measured from several CLSM images ($n = 100$). The aspect ratio of major axis/minor axis of the cells on the pristine Ti, **ANOD**, and **GMA-full** were 3.34 ± 2.69, 3.85 ± 3.02, and 5.93 ± 3.76, respectively (Fig. 9). Statistically significant differences between **GMA-full** and **ANOD** ($P < 10^{-4}$) and between **GMA-full** and pristine Ti ($P < 10^{-6}$) were observed in the measurement. Stem cells which present high aspect ratio morphologies are generally closer to bone differentiated cells. The exact mechanism of this phenomenon requires further study. But in previous literature [32], cell shape has been shown to have a great influence on the differentiation of stem cells. The paper says that cells having high aspect ratio and more contractility preferred to differentiate to osteoblasts than adipocytes. In our experiment, ADSCs incubated on the surface of **GMA-full** grew with higher aspect ratio, which indicates that the surface of **GMA-full** could promote differentiation towards osteoblasts.

3.7. Stability of polymer thin film

Stability of the polymer thin film was investigated by emplacement and removal test. GMA-coated fixtures were implanted into a bone extracted from a deceased pig and removed from the bone. The surface of the extracted fixtures were analyzed by SEM and XPS. Fig. 10 shows SEM images of the implant fixtures before and after implantation and Table 1 shows atomic chemical compositions from XPS analysis. As shown in Fig. 10, there was little

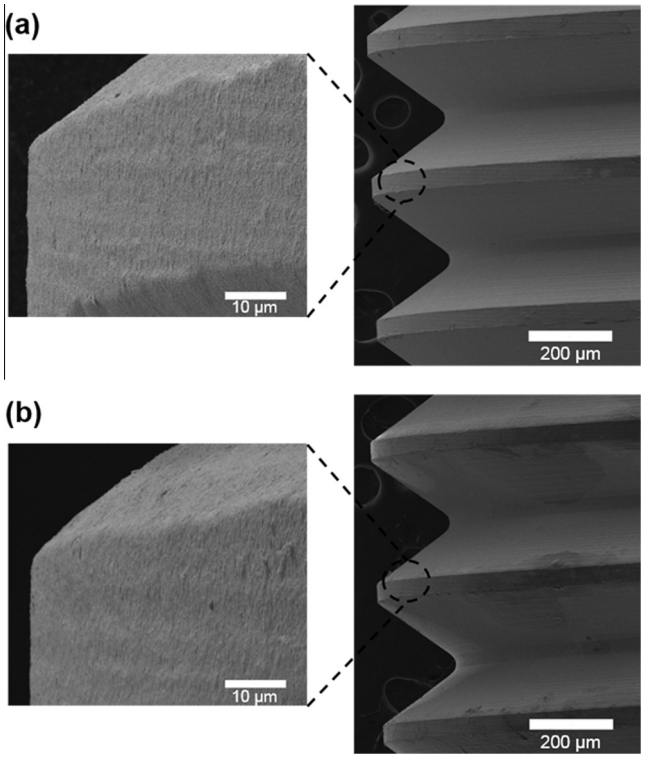

Fig. 10. FE-SEM micrographs of the GMA coated implant surface before implantation (a) and after implantation (b) into a bone of a deceased pig.

Table 1
Atomic chemical compositions of the surfaces of the **ANOD**, **GMA-full** (Before implantation) and **GMA-full** (after implantation) by XPS analysis.

Sample	% Ti	% C	% O
ANOD	19.8	19.4	60.8
GMA-full[a]			
Before implantation	1.5	67.7	30.8
GMA-full[b]			
After implantation	0.9 (1.6)	67.1 (11.8)	32.0 (10.3)
Fixture 1[c]	0.6 (0.8)	70.0 (8.3)	29.4 (7.6)
Fixture 2[c]	0.6 (0.7)	67.3 (9.1)	32.1 (8.4)
Fixture 3[c]	1.8 (3.0)	63.7 (19.4)	34.5 (16.4)

[a] C:O ratio of pGMA structure is 7:3.
[b] Average values of three fixtures (total 18 measurement).
[c] Average values of 6 measurements at different spots with standard deviations in parentheses.

difference between before insertion and after removal and the titanium surface nanostructures were also maintained. For further investigation, Titanium surfaces were characterized with XPS analysis (Table 1). While the chemical composition of **ANOD** was 19.81% Ti, 19.41% C, and 60.76% O, the composition of **GMA-full** were 1.52% Ti, 67.11% C, and 30.77% O, which implies that polymer thin films cover almost the entire implant fixture surface. The C:O ratio from the XPS analysis is similar to the predicted ratio from the molecular structure of pGMA (C:O ratio = 7:3). After GMA-coated fixtures were implanted to and removed from the bone, six different areas of the three fixtures were measured by XPS. The average compositions of **GMA-full** were 0.89% Ti, 67.11% C, and 32.01% O, which is similar to the sample before implantation. Among the three fixtures, polymer thin films of fixtures 1 and 2 were little damaged during the implantation process, but some parts of fixture 3 was moderately damaged. Overall, the polymer thin films displayed good mechanical stabilities during the implantation process.

In our experiments, the surface area of titanium was increased by anodization and furthermore functionalized by the introduced of epoxide units to the surface via deposition of functional polymer by iCVD. This method is very suitable and represents a promising technique to be applied to implants. This is because it is possible to generate thin films with high mechanical strength through crosslinking the polymer chains as well as the potential to introduce multiple functionalities such as surfaces that promote cell adhesion or have anti-bacterial/antifouling properties [7,33] via copolymerization [12].

4. Conclusion

We successfully fabricated a uniform, functional, polymer nanolayer using iCVD methods on a rough anodized Ti surface. GMA coated surfaces showed an increase in protein attachment for both fully coated and dot coated surfaces. This leads to increased ALP activity without cytotoxicity most notably with **GMA-dot** samples. We expect that the application of iCVD to the generation of functionalized implant surfaces provides the opportunity to introduce a variety of functional polymers onto these surfaces. Multi-functionality can be achieved by copolymerization as well as increased stability by crosslinking.

Acknowledgments

The authors would like to thank Biotem Co., Ltd. (Busan, Korea) for supplying titanium disks and implant fixtures. This work was supported by the National Research Foundation of Korea (NRF) grant funded by the Korea government (MEST) (NRF-2010-0019346), (NRF-2012-0008610), (NRF-2012R1A5A2051388).

References

[1] G.R. Parr, L.K. Gardner, R.W. Toth, J. Prosthet. Dent. 54 (1985) 410.
[2] K. Tanner, Eng. Med. 216 (2002) 215.
[3] L. Le Guéhennec, A. Soueidan, P. Layrolle, Y. Amouriq, Dent. Mater. 23 (2007) 844.
[4] C.N. Elias, Implant Dentistry – A Rapidly Evolving Practice, InTech, New York, 2011.
[5] F. Schwarz, M. Herten, M. Sager, M. Wieland, M. Dard, J. Becker, J. Clin. Periodontol. 34 (2007) 78.
[6] R.Z. LeGeros, Clin. Orthop. Rel. Res. 395 (2002) 81.
[7] T. Martin, S. Kooi, S. Chang, K. Sedransk, K. Gleason, Biomaterials 28 (2007) 909.
[8] W.E. Tenhaeff, K.K. Gleason, Adv. Funct. Mater. 18 (2008) 979.
[9] S.H. Baxamusa, S.G. Im, K.K. Gleason, Phys. Chem. Chem. Phys. 11 (2009) 5227.
[10] S.H. Baxamusa, K.K. Gleason, Chem. Vapor Depos. 14 (2008) 313.
[11] T.P. Martin, K.K. Lau, K. Chan, Y. Mao, M. Gupta, W. Shannan, Surf. Coat. Technol. 201 (2007) 9400.
[12] S.H. Baxamusa, K.K. Gleason, Adv. Funct. Mater. 19 (2009) 3489.
[13] W.S. O'Shaughnessy, M. Gao, K.K. Gleason, Langmuir 22 (2006) 7021.
[14] W. Lee, T. Oshikiri, K. Saito, K. Sugita, T. Sugo, Chem. Mat. 8 (1996) 2618.
[15] G. Yang, E. Kang, K. Neoh, J. Polym. Sci. Pol. Chem. 38 (2000) 3498.
[16] Y. Mao, K.K. Gleason, Langmuir 20 (2004) 2484.
[17] J. Liu, X. Wang, Q. Jin, T. Jin, S. Chang, Z. Zhang, A. Czajka-Jakubowska, W.V. Giannobile, J.E. Nör, B.H. Clarkson, Biomaterials 33 (2012) 5036.
[18] E. Monaco, M. Bionaz, S. Hollister, M. Wheeler, Theriogenology 75 (2011) 1381.
[19] J. Hall, J. Lausmaa, Appl. Osseointegration Res. 1 (2000) 5.
[20] X. Cui, H.-M. Kim, M. Kawashita, L. Wang, T. Xiong, T. Kokubo, T. Nakamura, Dent. Mater. 25 (2009) 80.
[21] M.-J. Kim, B. Lee, K. Yang, J. Park, S. Jeon, S.H. Um, D.-I. Kim, S.G. Im, S.-W. Cho, Biomaterials 34 (2013) 7236.
[22] S.E. Kim, S.-H. Song, Y.P. Yun, B.-J. Choi, I.K. Kwon, M.S. Bae, H.-J. Moon, Y.-D. Kwon, Biomaterials 32 (2011) 366.
[23] J. Chen, S. Mwenifumbo, C. Langhammer, J.P. McGovern, M. Li, A. Beye, W. Soboyejo, J. Biomed. Mater. Res. B Appl. Biomater. 82 (2007) 360.
[24] G. Zhao, Z. Schwartz, M. Wieland, F. Rupp, J. Geis-Gerstorfer, D. Cochran, B. Boyan, J. Biomed. Mater. Res., Part A 74 (2005) 49.
[25] L. Ponsonnet, K. Reybier, N. Jaffrezic, V. Comte, C. Lagneau, M. Lissac, C. Martelet, Mater. Sci. Eng., C 23 (2003) 551.
[26] J.H. Kim, S.D. Lee, J.M. Han, T.G. Lee, Y. Kim, J.B. Park, J.D. Lambeth, P.-G. Suh, S.H. Ryu, FEBS Lett. 430 (1998) 231.
[27] R. Olivares-Navarrete, S.L. Hyzy, D.L. Hutton, C.P. Erdman, M. Wieland, B.D. Boyan, Z. Schwartz, Biomaterials 31 (2010) 2728.
[28] H. Liao, A.-S. Andersson, D. Sutherland, S. Petronis, B. Kasemo, P. Thomsen, Biomaterials 24 (2003) 649.
[29] L. Le Guehennec, M.-A. Lopez-Heredia, B. Enkel, P. Weiss, Y. Amouriq, P. Layrolle, Acta Biomater. 4 (2008) 535.
[30] R. Olivares-Navarrete, P. Raz, G. Zhao, J. Chen, M. Wieland, D. Cochran, R. Chaudhri, A. Ornoy, B. Boyan, Z. Schwartz, Proc. Natl. Acad. Sci. 105 (2008) 15767.
[31] G.S. Stein, J.B. Lian, T.A. Owen, FASEB J. 4 (1990) 3111.
[32] K.A. Kilian, B. Bugarija, B.T. Lahn, M. Mrksich, Proc. Natl. Acad. Sci. 107 (2010) 4872.
[33] R. Yang, J. Xu, G. Ozaydin-Ince, S.Y. Wong, K.K. Gleason, Chem. Mat. 23 (2011) 1263.